

Ruthenium catalysts based on mesoporous aromatic frameworks for the hydrogenation of arenes

Anton Maximov¹ · Anna Zolotukhina¹ ·
Leonid Kulikov¹ · Yulia Kardasheva¹ ·
Eduard Karakhanov¹

Received: 9 October 2015 / Accepted: 20 November 2015
© Akadémiai Kiadó, Budapest, Hungary 2015

Abstract Novel catalysts consisting of ruthenium nanoparticles supported on diamond-like porous aromatic frameworks (PAFs) with 3 and 4 benzene rings in the edges have been synthesized with a narrow particle size distribution (0.85 and 1.10 nm respectively). Several techniques, such as N₂ physisorption, Fourier transform infrared spectroscopy, transmission electron microscopy, X-ray photoelectron spectroscopy, and solid-state nuclear magnetic resonance were used for characterizing the synthesized materials. The obtained catalysts appeared to be active in the hydrogenation of various aromatic substances (specific catalytic activity reached activities up to 2660 mol_(Sub) h⁻¹ mol_(Ru)⁻¹ in the case of phenol). Notably, a size-selective hydrogenation was observed for catalysts based on PAFs.

Keywords Catalysis · Ruthenium nanoparticles · Porous aromatic frameworks · Arenes · Size-selective hydrogenation

Introduction

A key advantage in catalysis is the ability of catalysts to change the selectivity of reactions. Control of selectivity in homogeneous catalysis is possible by formation of inclusion compounds of the substrate with hosts like the catalyst (e.g. complexes with cyclodextrins, calixarenes) [1, 2]. Molecular constraints in the inclusion complexes influence the substrate chemical reactivity, including chemo-, regio-, and

Electronic supplementary material The online version of this article (doi:10.1007/s11144-015-0956-7) contains supplementary material, which is available to authorized users.

✉ Eduard Karakhanov
kar@petrol.chem.msu.ru

¹ Department of Petroleum Chemistry and Organic Catalysis, Moscow State University, Leninskiye Gory 1-3, GSP-1, Moscow, Russian Federation 119991

stereoselectivity. In heterogeneous catalysis, the control of reaction selectivity is enabled by the formation of active sites in well-defined cavities of porous materials. Reactions occur in designed, reactor-like specific constraining environments of the support (e.g. zeolite or MOF) [3, 4].

The organic analogs of molecular sieves are polymers with regular structures. Among the latter, porous aromatic frameworks—a new class of organic polymers—are one of the most promising materials (Fig. 1). Due to their high surface area, regular rigid aromatic structure, thermal and chemical stability, relatively facile functionalization [5–8], these materials can be applied in gas storage [9], gas separation [10] and heterogeneous catalysis [11–13]. The confinement of an active center in the constrained environment of a PAF could influence its catalytic behavior and the selectivity of the process. In addition, it is possible to make metal particles with specific shapes and sizes that depend on the structure of PAF.

The porous structure of PAFs is highly dependent on the geometry and size of monomers as well as the synthetic method of PAFs [14, 15]. In this regard, the most efficient methods for PAF synthesis are Yamamoto [16, 17] and Suzuki cross-coupling reactions [18, 19], and the most promising monomers are molecules with tetrahedral geometry, for example different derivatives of tetraphenylmethane [13].

The application of PAFs consists of immobilizing the complexes of transition metals (Cu, Ir, Re, Rh) [13, 20, 21]. Only few studies have been devoted to the investigation of substrate selectivity and the regulation of nanoparticle (NP) size using PAFs [22, 23]. For example, two-dimensional phosphorus-based PAFs (PP-P,

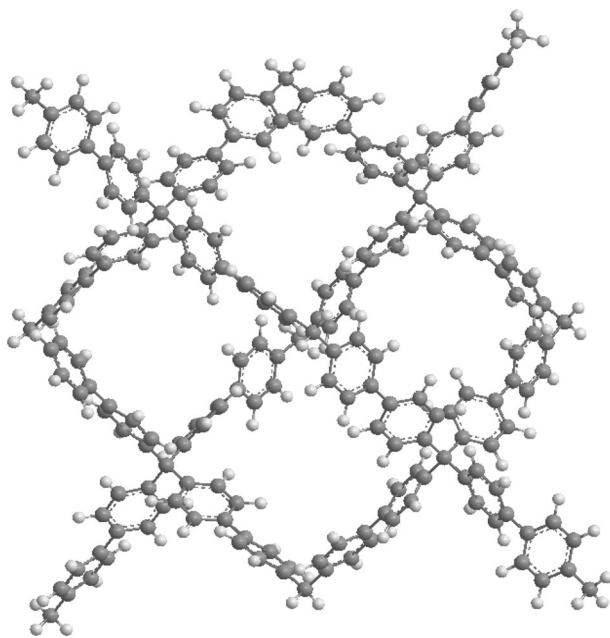


Fig. 1 Structure model of typical diamond-like porous aromatic framework

PP-PO) have been reported to support palladium NPs through the confinement of polymer and coordination of phosphorus to palladium, and excellent catalytic activity was shown in the Suzuki coupling reaction [24].

Herein we report the size-selective hydrogenation of aromatic compounds for Ru NP catalysts based on a PAF. We believe that the hydrophobic nature of the PAF surface will improve the transportation of aromatic substrate within the pores in comparison with conventional inorganic supports, such as zeolites. The rigid ordered structure of PAFs is expected to be a better stabilizer for Ru NPs than classical carbon supports. Porous polymer networks with 3 or 4 benzene rings in edge were synthesized by the Suzuki cross-coupling reaction between tetrahedral monomer (tetrakis (4-bromophenyl)methane) and 1,4-benzenediboronic or 4,4'-biphenyldiboronic acids. Specific surface area measurements and porosity analysis confirm mesoporous nature of PAFs. Ru NPs incorporated into these PAFs exhibited good catalytic performance in the hydrogenation of various aromatic substances. The catalysts demonstrate high substrate selectivity.

Experimental

Materials

All starting materials were purchased from commercial suppliers and used as received. The purification of solvents was performed according to standard methods. Tetrakis(4-bromophenyl)methane was synthesized via known literature procedure [25].

Synthesis of PAFs

General procedure: In a round bottomed flask equipped with the stir bar and silicone bath, tetrakis(4-bromophenyl)methane (1060 mg, 1.6677 mmol, 1 eq.) and 1,4-benzenediboronic acid (553 mg, 3.34 mmol, 2 eq.) were added to the mixture of 50 mL N,N'-dimethylformamide and 7 mL aqueous K_2CO_3 (2 mol/L). After 3 freeze–pump–thaw degassing cycles, $Pd(OAc)_2$ (38 mg, 0.167 mmol, 0.1 eq.) and PPh_3 (240 mg, 0.915 mmol, 0.55 eq.) were quickly added to the solution and degassed again by three freeze–thaw–pump cycles. The mixture was then heated at 140 °C and the reaction was stirred at this temperature for 24 h under static Ar atmosphere. After cooling to room temperature, the residue was filtered and washed with THF (4 × 50 mL), $CHCl_3$ (4 × 50 mL), EtOH (4 × 50 mL) and water (4 × 50 mL) and dried in vacuo to give PAF-20 as off-white powder (720 mg, 94 %).

Preparation of catalysts

General procedure

A mixture of $RuCl_3$ (50 mg), 1,5-cyclooctadiene (5 mL) and PAF material (250 mg) in MeOH (20 mL) was stirred at 40 °C for 4 h and then cooled to room

temperature. A solution of NaBH_4 (1 g) in MeOH (10 mL) was added dropwise with stirring. The resulting mixture was stirred at room temperature for 12 h and then the precipitate formed was filtered, washed with THF (2×30 mL) and EtOH (2×30 mL) and dried in vacuo to give Ru-PAFs as grey powder.

Hydrogenation reactions

General procedure

Catalytic reactions were performed in a steel reactor (4 ml) equipped with glass test-tube (aprox. 4 ml) and stir bar (vol. 0.2 ml). The stir bar, the catalyst (3 mg), the required amounts of aromatic substrate (1:2000 equiv. Ru per arene mol) and water (1:1 mass or volume) were introduced into the test-tube. Then the test-tube was inserted into the reactor and was sealed and pressurized with H_2 at the demanded pressure. The mixture was stirred at 80 °C and after the hydrogenation reaction was finished, the reactor was cooled down and depressurized. Conversions and selectivities were measured by gas chromatographic analysis.

Analysis

Fourier transform infrared spectra (FTIR) spectra were taken with a *Nicolet IR2000* (Thermo Scientific) instrument using multiple distortion of the total internal reflection method with multi-reflection HATR accessories, containing a ZnSe crystal 458 for different wavelengths with a resolution of 4 cm^{-1} in the range of $4000\text{--}400\text{ cm}^{-1}$. All spectra were taken by averaging 100 scans.

The solid state NMR spectra were measured on a *Varian NMR Systems* instrument with a resonance frequency of 500 MHz for ^1H magic angle spinning (MAS) NMR spectra and 125 MHz for ^{13}C cross polarization (CP) MAS NMR spectra in an impulse mode at a spinning speed of 10 kHz.

Specific surface area measurements and porosity analysis were performed using nitrogen adsorption–desorption isotherms at 77 K on a *Micromeritics Gemini VII 2390 V1.02t* apparatus using the BET method for surface area calculation and the BJH technique for average pore size and pore volume calculations. Prior to the analysis, the samples were dried at 100 °C under high vacuum for 8 h.

For transmission electron microscopy (TEM), a *LEO912 AB OMEGA* microscope with electron tube voltage of 100 kV was used.

X-ray photoelectron spectroscopy (XPS) analysis was performed on a *Kratos Axis Ultra DLD*. To excite photoelectrons, aluminum anode X-ray radiation was used ($\text{Al K}_\alpha = 1486.6\text{ eV}$) with a tube voltage of 12 kV and emission current of 20 mA. The calibration of photoelectron peaks was performed along the C1 s line with binding energy of 284.5 eV.

The metal content was analyzed by spectrophotometry on an *Agilent UV/Vis. 8453* instrument as $[\text{Ru}(\text{phen})]^{2+}$ complexes with preliminary sample preparation as described earlier [26].

GC analyses were carried out with a *ChromPack CP9001* apparatus equipped with FID and a semi-polar SE-30 100 % dimethylpolysiloxane column ($30\text{ m} \times 0.2\text{ mm}$

ID, 0.2 μm film); nitrogen as a carrier gas; flow rate 30 mL/min. Other parameters are shown in the Supplementary Information (Table S5).

Results and discussion

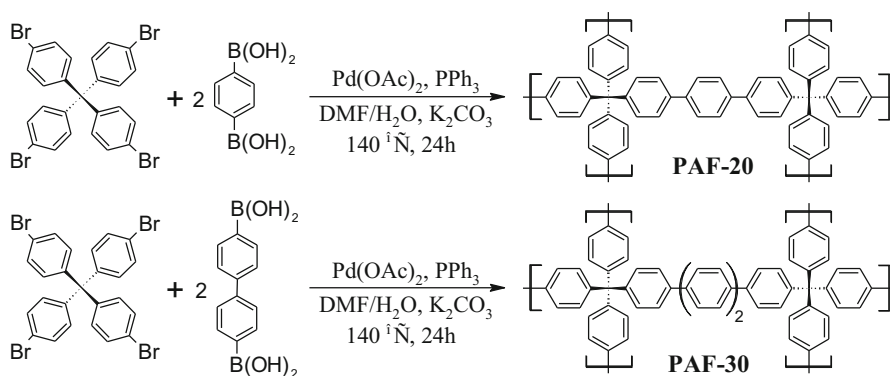
Synthesis and characterization of PAFs

PAF-20 and PAF-30, containing 3 and 4 benzene rings in edge, respectively, were synthesized by the Suzuki cross-coupling reaction between tetrakis(4-bromophenyl)methane and 1,4-benzenediboronic and 4,4'-biphenyldiboronic acids (Scheme 1).

The IR spectra of both frameworks (Fig. 2) showed the strong δ_{oop} C–H band at 808 cm^{-1} and less intensive $\nu\text{C}=\text{C}_{\text{p-Ar}}$ and $\delta_{\text{ip}}\text{C}_{\text{sp}^3}\text{--C}_{\text{Ar}}$ bands at 1485 and 1005 cm^{-1} , respectively. The absence of B–OH bands at 3370 cm^{-1} and C–Br band at 1076 cm^{-1} in the spectra of PAFs confirms the almost complete conversion of monomers to the final product in coupling reaction.

Because structural information from FTIR spectra is limited, an investigation by means of solid-state ^{13}C CP/MAS NMR spectroscopy was done (Fig. 3). A group of signals with a chemical shift in the range of 120–150 ppm could be observed. The most intensive signal at 129 ppm corresponds to remoted from the central $\text{sp}^3\text{--C}$ atom unsubstituted carbon atoms in benzene rings, since these C atoms are directly connected to protons and thus cross polarization is stronger; the signal at 66 ppm can be attributed to a quaternary carbon atom.

Assuming that the relative intensities of signals depend on the number of similar C atoms and their screening, the signal at 141 ppm could correspond to substituted phenyl carbon atoms, which linked one with another, and signals at 132 and 147 ppm could be attributable to unsubstituted and substituted carbon atoms in the nearest to central $\text{sp}^3\text{--C}$ atom benzene ring. This result is in agreement with the work reported by Yuan et al. [27], who observed similar spectrum of PAF-30. Similarly to



Scheme 1 Synthesis of PAF-20 and PAF-30

IR-PAF-3.0.esp

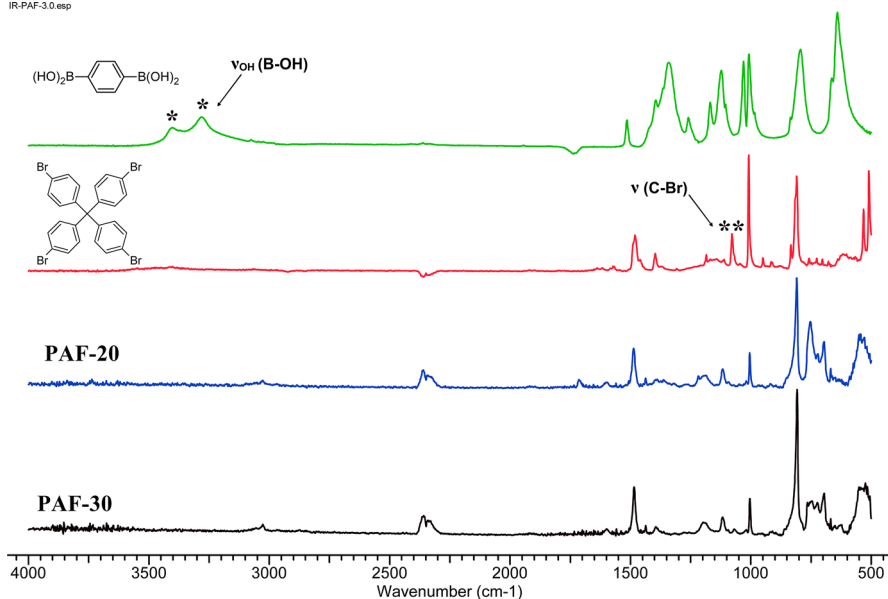


Fig. 2 FTIR spectra of 1,4-phenylenediboronic acid, tetrakis (4-bromophenyl)methane, PAF-20 and PAF-30

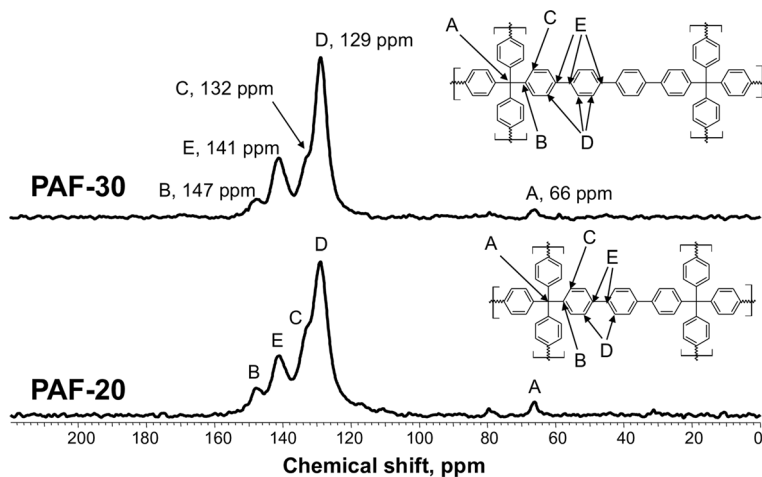


Fig. 3 Solid-state ^{13}C CP/MAS NMR spectra of frameworks PAF-20 and PAF-30

the results of the FTIR analysis, signals attributed to halogen or boronic acid, are absent in ^{13}C CP/MAS NMR spectra of frameworks.

The corresponding frameworks were characterized by BET (Table 1). Despite the fact that the isotherms are not close, it is possible to calculate both surface area and average pore diameter [27]. Both PAFs exhibited mesoporous properties:

distinct hysteresis extending to low pressure between the adsorption and desorption cycles (Fig. 4; Fig. S2, S3 is the Supplementary Information) confirms mesoporous nature of PAFs. In accordance with the theory, with increasing the edge length decline of surface area is observed.

To explore the morphology of PAFs, TEM analysis was performed. The micrographs (Fig. S4, Supplementary Information) show that the frameworks consists of 150–250 nm-sized spheres and their agglomerates.

Synthesis and characterization of catalysts

The synthesis of Ru nanoparticles was performed within the pores of corresponding frameworks through the impregnation of PAFs with ruthenium salt and subsequent reduction with sodium borohydride (Scheme 2).

Only about half of the ruthenium was introduced into the pores (4.83 wt% for Ru-PAF-30 and 3.86 wt% for Ru-PAF-20). This fact could be explained by washing up of some Ru during the process of reduction. The ruthenium content in Ru-PAF-30, however, is in good agreement with the experimental data of porosity analysis. The PAF-30 pore volume is 1.34 times more than in case of PAF-20 (Table 1) and the quantity of Ru in Ru-PAF-30 is 1.25 times more than in Ru-PAF-20.

While ruthenium incorporates into the PAF pores, the surface area of material decreases. However, the degree of such decreasing correlates with the amount of introduced metal. For instance, if the metal content in the material is more than 10 %, the surface area decreases dramatically [20, 24, 28]. In contrast, when the metal content is 5 % or less, this decreasing is insignificant [20]. Therefore, we except only a slight decrease of surface area (approximately 10 % decrease from original PAFs) in both Ru-PAF-30 and Ru-PAF-20.

In the solid-state ^{13}C CP/MAS NMR spectra of Ru-PAFs (Fig. 5), signals of all carbon atoms are similar to those in the original frameworks. The small decreasing of the relative intensities of signals at 132, 141 and 147 ppm can be attributed to structure deformation and screening that arises under the introduction of Ru NPs. Similar results were obtained earlier for Ru NPs in MOF-5 [29] and Pd NPs in 1,2,3-triazolyl-containing POPs [23].

In the TEM and HRTEM images of both Ru-PAF-20 and Ru-PAF-30 (Fig. 6), unimodal distribution of Ru NP sizes can be observed. The average NP sizes are 0.9 ± 0.2 and 1.2 ± 0.2 nm for Ru-PAF-20 and Ru-PAF-30, which reveals distinct correlation between the edge length/pore volume and NP sizes.

XPS analysis exhibits that both Ru-PAF-20 and Ru-PAF-30 are composed of C, O and Ru; any presence of bromine, boron or palladium was not detected (Table S6,

Table 1 Pore properties of PAF-20 and PAF-30

| Framework | S_{BET} (m^2/g) | Av. pore size (\AA) | Pore vol. (cm^3/g) |
|-----------|--------------------------------------------|--------------------------------|--------------------------------------|
| PAF-20 | 403 | 36 | 0.26 |
| PAF-30 | 240 | 75 | 0.35 |

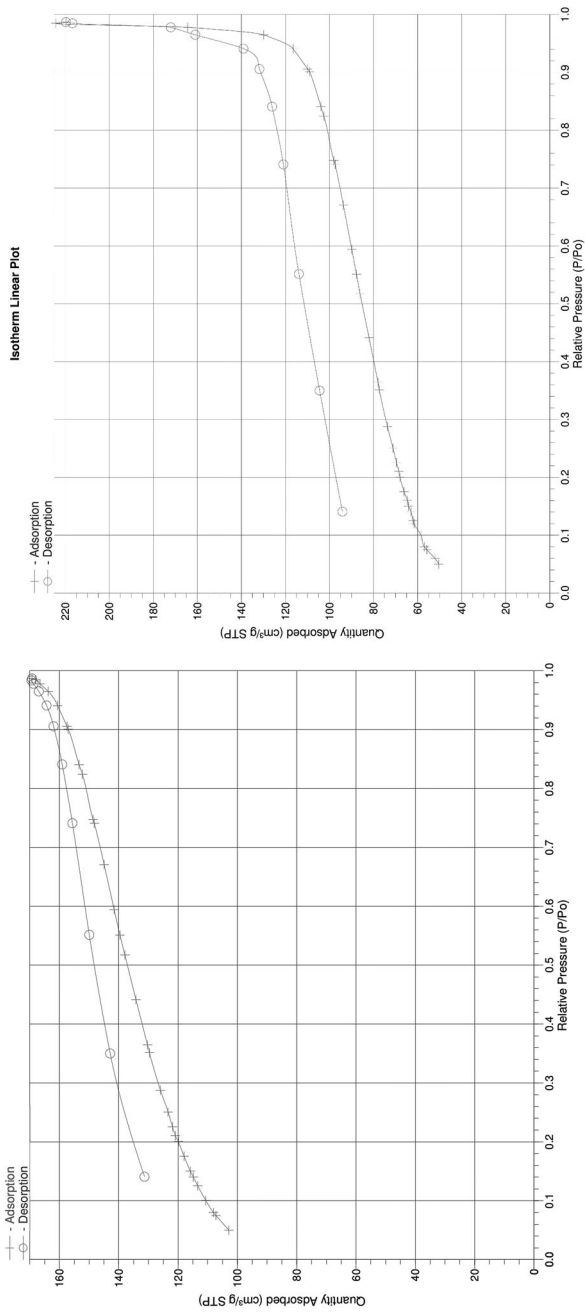
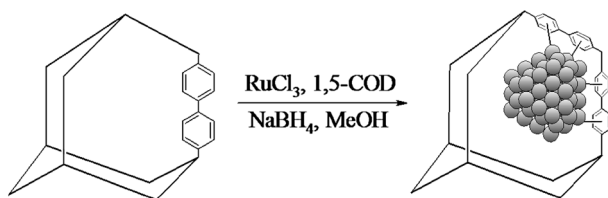


Fig. 4 N₂ adsorption isotherms of PAF-20 (*left*) and PAF-30 (*right*) measured at 77 K



Scheme 2 Immobilization of Ru NPs into PAF-20 and PAF-30

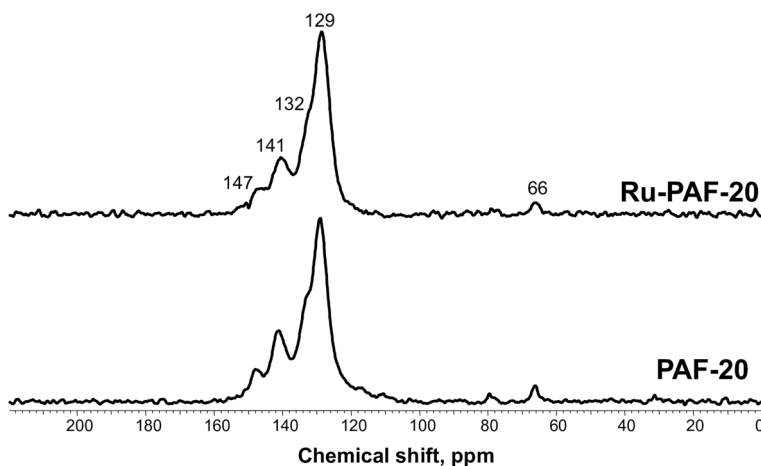


Fig. 5 Solid-state ^{13}C CP/MAS NMR spectrum of PAF-20 and Ru-PAF-20

Supplementary Information). The peak positions were corrected by the C1 s peak at 284.6 eV. In both spectra, two sets of doublet peaks corresponding to RuO_2 (Ru $3d_{5/2}$, signals at 281.6 and 285.8 eV) and $\text{RuO}_2 \cdot x\text{H}_2\text{O}$ (Ru $3d_{5/2}$, signals at 282.1.7 and 286.9 eV) [30] can be observed (Fig. 7), confirming incorporation of ruthenium into PAFs' pores. The absence of Ru^0 could be explained through ease of ruthenium oxidation by air oxygen [26].

Catalysis

The catalytic activity of Ru-PAF-20 and Ru-PAF-30 was investigated in the hydrogenation of aromatic substances. Reactions were carried out at 80 °C and different (30 or 10 bar) P_{H_2} at near to 1:2000 Ru to arene ratio.

Despite the common usage of conception of turnover frequency (TOF) in describing catalytic performances nowadays, we did not apply it in the current work due to the fact that its utility and accuracy are debated at present [31–33]. The conception of the initial reaction rate per quantity of ruthenium on the surface of NPs was used (equations are presented in the Supplementary Information). We

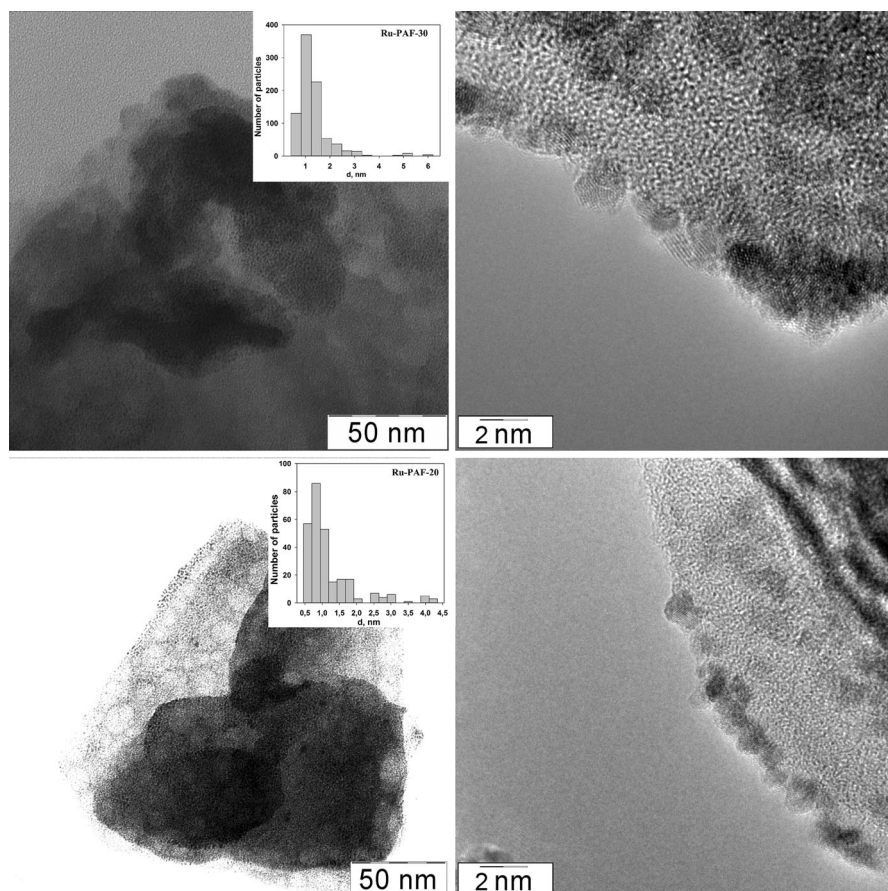


Fig. 6 TEM and HRTEM images of Ru-PAF-30 (*top*) and Ru-PAF-20 (*bottom*); 50 nm scale resolution in TEM images and 2 nm scale resolution in HRTEM images

make the assumptions that hydrogenation mechanisms on the surface of Ru NPs are similar for all arenes, the reactions are first order with respect to hydrogen due to its low solubility and zeroth order with respect to arenes because of the high value of arene:Ru ratio (see phenol hydrogenation, Fig. 10). This allows us to compare catalytic performances of Ru-PAF-20 and Ru-PAF-30 without determining the rate laws.

The main catalytic results in the hydrogenation of alkylbenzenes, tetralin and phenol for Ru-PAF-30 and Ru-PAF-30 are summarized in Fig. 8 and Table S7. The primary reaction products were the corresponding derivatives of cyclohexane. An observable decline of catalytic activity in the order benzene-toluene-tetralin could be explained by increasing the diffusion limitations due to increasing of the substrate size. It should be mentioned that such decline is much more substantial in the case of Ru-PAF-20. As shown in Fig. 8, Ru-PAF-20 was active only in the hydrogenation of substrates with small molecule sizes: the conversion of tetralin

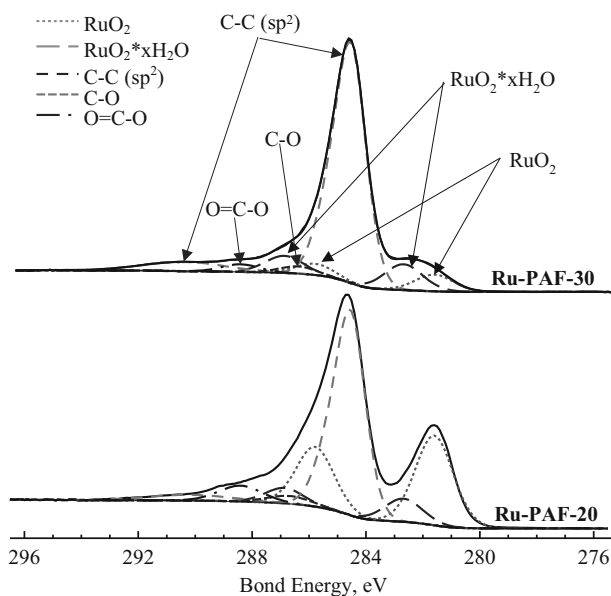


Fig. 7 XPS measurements for Ru-PAF-20 (*bottom*) and Ru-PAF-30 (*top*)

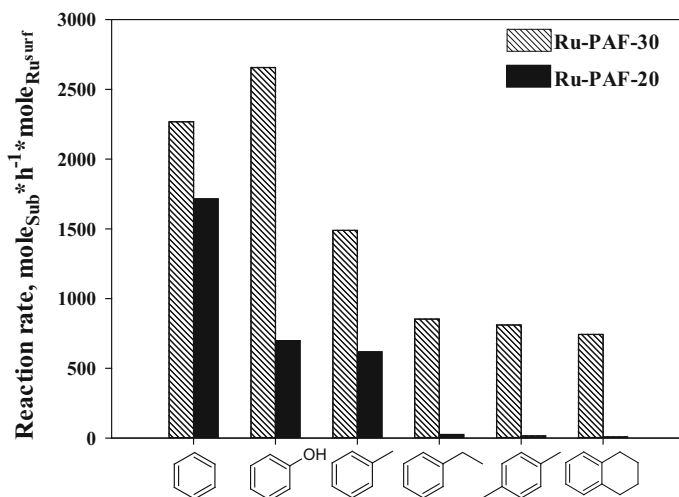


Fig. 8 Hydrogenation of arenes in presence of Ru-PAF-20 and Ru-PAF-30. Reaction conditions: 80 °C, 30 bar H₂, 1 h, 3 mg cat., V(H₂O) = V(sub.); Ru:arene = 1:2000 mol

hydrogenation on Ru-PAF-30 was about 30 % after 1 h whereas the conversion on Ru-PAF-20 was not more than 2 %.

Close values of reaction rate for ethylbenzene, *p*-xylene and tetralin in case of Ru-PAF-30 are in accordance with the molecule sizes.

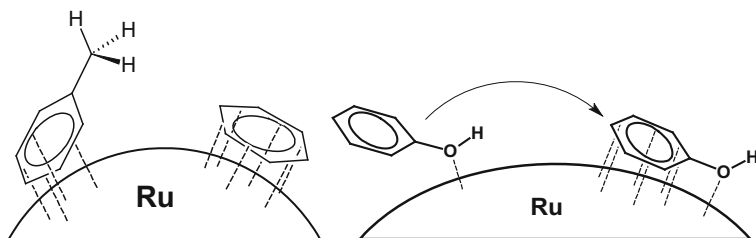
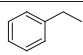
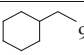
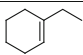
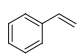
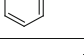
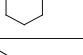
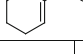
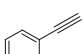
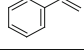
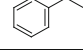
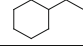


Fig. 9 Different adsorption mechanisms on Ru NPs for benzene, toluene and phenol

Table 2 Performance of Ru-PAF-30 in the hydrogenation of C2-substituted benzenes

| Substrate | Sub./Ru ratio | Conv., % | Reaction rate*, $\frac{\text{mol}_{(\text{H}_2)}}{\text{h}^{-1} \text{mol}_{(\text{Ru})}^{-1}}$ | Products distribution | |
|-----------------------------------------------------------------------------------|---------------|----------|----------------------------------------------------------------------------------------------------|---------------------------------------------------------------------------------------|---------------------------------------------------------------------------------------|
|  | 2038 | 36% | 2515 |  95% |  5% |
|  | 1928 | 100% | 5725 |  48% |  50% |
| | | | |  2% | |
|  | 2150 | 100% | 3496 |  67% |  31% |
| | | | |  2% | |

Reaction conditions: 80 °C, 30 bar H_2 , 1 h, 3 mg cat., $V(\text{H}_2\text{O}) = V(\text{sub.}) = 300 \mu\text{L}$

^a Reaction rates calculations were based on hydrogen conversion

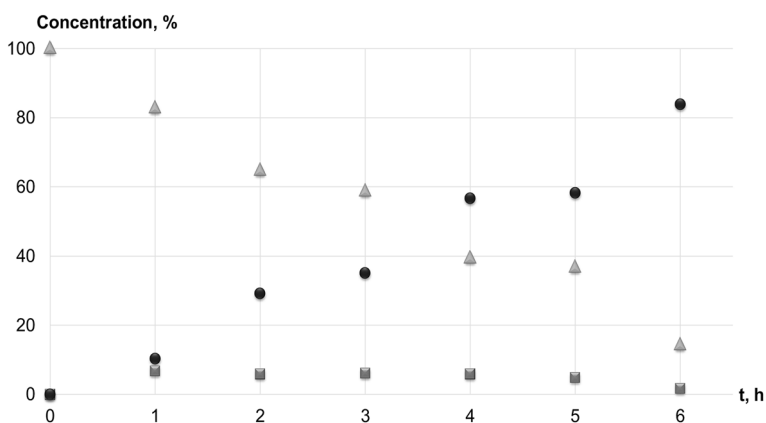


Fig. 10 Concentration distribution in the hydrogenation of phenol. Triangles phenol, circles cyclohexanol, squares cyclohexanone. Reaction conditions: 80 °C, 10 bar H_2 , 1 h, 3 mg cat., H_2O (300 μL), PhOH 300 mg

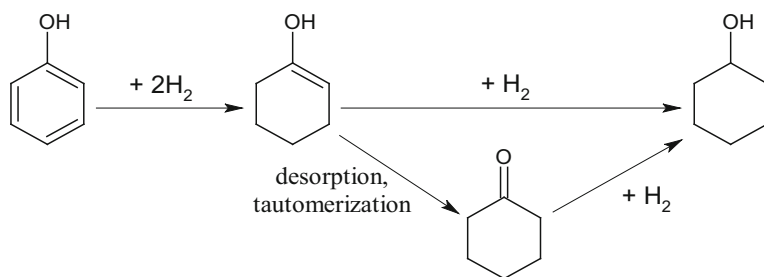


Fig. 11 The scheme of phenol hydrogenation

Ru-PAF-30 showed higher activity in the hydrogenation of phenol in comparison with benzene and toluene, probably because of special adsorption character of these substances.

In the case of benzene and toluene only parallel π -adsorption could take place, while the adsorption of phenol occurs by a complicated mechanism, including the interaction of the polar OH-phenol group with the ruthenium surface and subsequent π -adsorption of benzene ring (Fig. 9). Since the Ru–O interaction is stronger than Ru–(η^6 -arene), the adsorption of phenol occurs easier and thus the activity of Ru-PAF-30 in the hydrogenation of phenol is higher. However, when Ru-PAF-20 was employed as a catalyst, reaction rates were close for phenol and toluene, confirming the domination of steric factors in the reaction.

On the basis of these results, a further investigation of catalytic performances of Ru-PAF-30 was performed. As shown in Table 2, the catalyst was active in the hydrogenation of all C2-substituted benzenes; the hydrogenation rate of styrene was much faster than ethylbenzene and phenylacetylene, which probably resulted from the coordination of styrene to the Ru NP surface by both of plane of the benzene ring and C=C bond due to their conjugation. In the case of phenylacetylene hydrogenation, the products were ethylbenzene and styrene, according to the higher reactivity of acetylene group than benzene ring.

In order to study the kinetics of phenol hydrogenation, the H_2 pressure was reduced to 10 bar. We observed low alcohol/ketone ratio only in the beginning of reaction. Then the cyclohexanone quantity was about 6 % up to the 6 h of reaction and the alcohol was the main product for Ru catalysts based on PAF (Fig. 10). It is believed that phenol is first hydrogenated into cyclohexanone, and subsequently cyclohexanone. The reaction includes phenol conversion to the corresponding cyclohexenol, which can desorb from the metal surface and transform to cyclohexanone (Fig. 11) or undergo further hydrogenation to cyclohexanol. Cyclohexanol is the main product when the hydrogenation rate significantly exceeds desorption rate. In contrast, when desorption predominates, the yield of cyclohexanone is remarkable. At longer reaction times, cyclohexanone can then be further hydrogenated to form cyclohexanol [34].

Conclusions

The use of porous aromatic frameworks as support to get heterogeneous Ru-containing catalysts has been described. The material obtained is characterized by homogeneous distribution of Ru NPs by PAFs volume and narrow size distribution. The pore size and volume of PAFs severely affected the size of particles and the quantity of the Ru in catalysts. The particle size and quantity of Ru was higher for PAF-30. Both Ru-PAF-20 and Ru-PAF-30 exhibit good catalytic activities in the hydrogenation of arenes, and the influence of the original framework on the substrate selectivity of catalysts was demonstrated. The activity of catalyst based on the support with smaller pores (PAF-20) was negligible for bulk substrates.

Acknowledgments The study was supported by the Russian Science Foundation within a framework of Project N 15-19-00099.

References

1. Maksimov AL, Sakharov DA, Filippova TY, Zhuchkova AY, Karakhanov EA (2005) *Ind Eng Chem Res* 44(23):8644–8653
2. Karakhanov EA, Karapetyan LM, Kardasheva YS, Maksimov AL, Runova EA, Terenina MV, Filippova TY (2008) *Macromol Symp* 270:106–116
3. Brinker UH, Miesusset JL (2010) *Molecular encapsulation: organic reactions in constrained systems*. Wiley, New York
4. Peters R (2015) *Cooperative catalysis: designing efficient catalysts for synthesis*. Wiley, New York
5. Merino E, Verde-Sesto E, Maya EM, Corma A, Iglesias M, Sanchez F (2014) *Appl Catal A: Gen* 469:206–212
6. Jiang JX, Su F, Trewin A, Wood CD, Campbell NL, Miu H, Dickinson C, Ganin AY, Rosseinsky MJ, Khimyak YZ, Cooper AI (2007) *Angew. Chem.* 119:8728–8732
7. Jiang JX, Su F, Trewin A, Wood CD, Campbell NL, Miu H, Dickinson C, Ganin AY, Rosseinsky MJ, Khimyak YZ, Cooper AI (2007) *Angew Chem Int Ed* 46:8574–8578
8. Yuan S, Dorney B, White D, Kirklin S, Zapol P, Yu L, Liu DJ (2010) *Chem Commun* 46:4547–4549
9. Murray LJ, Dinca M, Long JR (2009) *Chem Soc Rev* 38:1294–1314
10. Li JR, Ryan JK, Zhou HC (2009) *Chem Soc Rev* 38:1477–1504
11. Lee J, Farha OK, Roberts J, Scheidt KA, Nguyen ST, Hupp JT (2009) *Chem Soc Rev* 38:1450–1459
12. Kaur P, Hupp JT, Nguyen ST (2011) *ACS Catal* 1:819–835
13. Verde-Sesto E, Pintado-Sierra M, Corma A, Maya EM, de la Campa JG, Iglesias M, Sanchez F (2014) *Chem Eur J* 20:5111–5120
14. Holst JR, Stöckel E, Adams DJ, Cooper AI (2010) *Macromolecules* 43:8531–8538
15. Jiang JX, Su F, Trewin A, Wood CD, Niu H, Jones JTA, Khimyak YZ (2008) *J Am Chem Soc* 130(24):7710–7720
16. Schmidt J, Werner M, Thomas A (2009) *Macromolecules* 42:4426–4429
17. Ben T, Ren H, Ma S, Cao D, Lan J, Jing X, Wang W, Xu J, Deng F, Simmons JM, Qiu S, Zhu G (2009) *Angew Chem Int Ed* 48:9457–9460
18. Chen L, Honsho Y, Seki S, Jiang D (2010) *J Am Chem Soc* 132:6742–6748
19. Weber J, Thomas A (2008) *J Am Chem Soc* 130(20):6334–6335
20. Fritsch J, Drache F, Nickerl G, Böhlmann W, Kaskel S (2013) *Microporous Mesoporous Mat* 172:167–173
21. Jiang JX, Wang C, Laybourn A, Hasell T, Clowes R, Khimyak YZ, Xiao J, Higgins SJ, Adams DJ, Cooper AI (2011) *Angew Chem Int Ed* 50:1072–1075
22. Zhang P, Qiao ZA, Jiang X, Veith GM, Dai S (2015) *Nano Lett* 15:823–828
23. Li L, Zhao H, Wang R (2015) *ACS Catal* 5(2):948–955
24. Zhang Q, Yang Y, Zhang S (2013) *Chem Eur J* 19:10024–10029
25. Lu J, Zhang J (2014) *J Mater Chem A* 2:13831–13834

26. Maximov A, Zolotukhina A, Murzin V, Karakhanov E, Rosenberg E (2015) *ChemCatChem* 7:1197–1210
27. Yuan Y, Sun F, Ren H, Jing X, Wang W, Ma H, Zhao H, Zhu G (2011) *J Mater Chem* 21:13498–13502
28. Zhang Q, Zhang S, Li S (2012) *Macromolecules* 45:2981–2988
29. Schröder F, Esken D, Cokoja M, van den Berg MWE, Lebedev OI, Van Tendeloo G, Walaszek B, Buntkowsky G, Limbach HH, Chaudret B, Fischer RA (2008) *J Am Chem Soc* 130(19):6119–6130
30. Shen JY, Adnot A, Kaliaguine S (1991) *Appl Surf Sci* 51:47–60
31. Kozuch S, Martin JML (2012) *ACS Catal* 2:2787–2794
32. Lente G (2013) *ACS Catal* 3:381–382
33. Crooks AB, Yih KH, Li L, Yang JC, Özkar S, Finke RG (2015) *ACS Catal* 5:3342–3353
34. Maksimov AL, Kuklin SN, Kardasheva YS, Karakhanov EA (2013) *Petroleum Chem* 53(3):177–184